He, T. and Zhu, M. and Mills, B. and Wynn, P. and Zhuravlev, A. and Tostevin, R. and Pogge von Strandmann, Philip A.E. and Yang, A. and Poulton, S. and Shields, G. (2019) Possible links between extreme oxygen perturbations and the Cambrian radiation of animals. Nature Geoscience 12 , pp. 468-474. ISSN 1752-0894.

Extreme oxygen perturbations regulated the Cambrian radiation of animals

Tianchen He[1,2]*, Maoyan Zhu[3,4], Benjamin J.W. Mills[2], Peter M. Wynn[5], Andrey Yu. Zhuravlev[6], Rosalie Tostevin[7], Philip A. E. Pogge von Strandmann[1], Aihua Yang[8], Simon W. Poulton[2], Graham A. Shields[1]

[1]London Geochemistry and Isotope Centre (LOGIC), Institute of Earth and Planetary Sciences, University College London and Birkbeck, University of London, London, WC1E 6BT, UK

[2]School of Earth and Environment, University of Leeds, Leeds, LS2 9JT, UK.

[3]State Key Laboratory of Palaeobiology and Stratigraphy & Center for Excellence in Life and Paleoenvironment, Nanjing Institute of Geology and Palaeontology, Chinese Academy of Sciences, Nanjing, 210008, China.

[4]College of Earth Sciences, University of Chinese Academy of Sciences, Beijing, 100049, China.

[5]Lancaster Environment Centre, Lancaster University, Lancaster, LA1 4YQ, UK.

[6]Department of Biological Evolution, Faculty of Biology, Lomonosov Moscow State University, Leninskie gory 1(12), Moscow 119234, Russia.

[7]Department of Earth Sciences, University of Oxford, Oxford, OX1 3AN, UK.

[8]State Key Laboratory for Mineral Deposits Research, School of Earth Sciences and Engineering, Nanjing University, Nanjing, 210093, China.

*e-mail: T.He@leeds.ac.uk

The role of oxygen as a driver for early animal evolution is widely debated. During the Cambrian explosion, episodic radiations of major animal phyla occurred coincident with repeated carbon isotope fluctuations. However, the driver of these isotope fluctuations and potential links to environmental oxygenation are unclear. Here, we report high-resolution carbon and sulphur isotope data for marine carbonates from the south-eastern Siberian Platform, which documents the canonical explosive phase of the Cambrian radiation from ~524 to ~514 Myr ago. These analyses demonstrate a strong positive covariation between carbonate $\delta^{13}C$ and carbonate-associated sulphate $\delta^{34}S$ through five isotope cycles. Biogeochemical modelling suggests that this isotopic coupling reflects periodic oscillations in atmospheric O_2 and the extent of shallow ocean oxygenation which, remarkably, directly coincides with episodic maxima in biodiversity of animal phyla. Conversely, the subsequent Botoman–Toyonian animal extinction events (~514 to ~512 Myr ago) coincided with decoupled isotope records that suggest a shrinking marine sulphate reservoir and expanded

shallow marine anoxia. These observations demonstrate that fluctuations in oxygen availability in the shallow marine realm exerted a primary control on the timing and tempo of biodiversity radiations at a crucial phase in the early history of animal life.

The early Cambrian witnessed a dramatic diversification of animal body plans and behaviours[1], **as well as between-species interactions and palaeocommunity innovations[2,3],** ultimately leading to modern animal **ecosystems**. Ocean oxygenation is a commonly invoked environmental pre-requisite[4–6]. However, some recent studies suggest that despite probable low-oxygen conditions, the oceans exceeded requisite oxygen thresholds for simple animals, such as sponges, well before the Cambrian Period[7,8]. **Many of the new animal body plans and lifestyles that appeared during the early Cambrian are associated with considerably higher oxygen demands[9,10]. Fluctuations in the maximum dissolved oxygen content of surface waters, or the extent of shallow ocean oxygenation, could therefore have played an important role in regulating the pattern of Cambrian radiations.** This brings into question the role of oxygen in early animal evolution, which is exacerbated by a lack of convincing evidence for a direct link between Earth's oxygenation history and early Cambrian bio-radiations and extinctions.

High-resolution records of the sulphur and carbon cycles, when considered in the context of the fossil record may, however, afford an opportunity to resolve **potential** environmental controls on early animal evolution. The marine biogeochemical sulphur and carbon cycles interconnect via their respective redox-sensitive reservoirs and fluxes. Both elements have a single, large oxidised oceanic reservoir (dissolved sulphate and inorganic carbon, respectively), the isotopic composition of which is governed by isotope fractionation during **microbially**-mediated reduction to sulphide (ultimately preserved as pyrite) and organic carbon, respectively. Burial of these reduced species represents the two main net sources of oxygen to the surface environment[11–13], and also imprints on both the seawater sulphate sulphur isotope ($\delta^{34}S$, as recorded by carbonate-associated sulphate) and carbon isotope ($\delta^{13}C$, as recorded in carbonate) records, allowing redox changes in the surface environment to be traced through geologic time.

Here we present paired carbon and sulphur isotope data from lower Cambrian marine carbonates of the south-eastern Siberian Platform. These data provide a continuous, high-resolution record from Cambrian Stage 2 through to Stage 4 (~524-512 Myr ago; Fig. 1), and allow a direct assessment of potential links between ocean redox variability, atmospheric oxygenation, and the major biological events of the early Cambrian.

Carbon and sulphur isotope systematics

Carbonate-carbon and carbonate-associated sulphate sulphur isotope analyses (see Methods) were performed on well-preserved samples collected from sections along the Aldan and Lena rivers in Siberia. **These precise sections archive a continuous and highly fossiliferous sedimentary record from a shallow, open ocean carbonate platform, and preserve over half of all fossil forms currently known from the Cambrian radiation interval worldwide, thus providing a unique window into early Cambrian shallow marine ecosystems** (see Supplementary Information for geological and palaeontological context, sample details, and all data).

Our carbon isotope data **record** five cycles through Stage 2 and Stage 3 of the lower Cambrian**. Positive excursions are** labelled here as III to VII (Fig. 1), consistent with previous studies of the Siberian Platform[14,15] **but these excursions are also found** elsewhere[16,17]. The new sulphur isotope data range from +16‰ to +36‰, demonstrating that seawater sulphate $\delta^{34}S$ fell from **a peak** (~40-45‰) during the late Ediacaran[18,19] to lower values **by** the early Cambrian. Significantly, however, these data also demonstrate for the first time that oceanic sulphate $\delta^{34}S$ varied across five cycles that directly correlate with ~~the~~ excursions in seawater $\delta^{13}C$ (Fig. 1; see Supplementary Table S1 for statistical correlation parameters). In sharp contrast to the coupled $\delta^{13}C$-$\delta^{34}S$ trends during the Cambrian stages 2-3, the $\delta^{34}S$ trend across the early Cambrian Stage 4 Botoman–Toyonian extinctions (BTE; the first animal mass extinction of the Phanerozoic Eon)[20,21] is characterised by rapid fluctuations of large magnitude that are decoupled from the carbon isotope record (Fig. 1).

Over long timescales the excess oxidant generated by increased organic carbon burial (as indicated by higher carbonate $\delta^{13}C$) may be balanced by reduced rates of pyrite burial (lower seawater sulphate $\delta^{34}S$), and vice-versa, which results in **relatively stable atmospheric**

oxygen levels and an inverse relationship between the first-order **global** seawater $\delta^{13}C$ and $\delta^{34}S$ records[22,23]. However, the positive correlations we observe between $\delta^{13}C$ and $\delta^{34}S$ in ~~the~~ Cambrian stages 2-3 likely reflect **higher rates of both organic carbon and pyrite sulphur burial, which would be associated with large** distinct pulses in **atmospheric** oxygenation, as previously suggested for the late Cambrian SPICE (Steptoean Positive C-isotope Excursion) event[13].

The rate of change of seawater sulphate sulphur isotope ratios allows us to estimate marine sulphate concentrations through this interval. Using the 'rate method' model[24,25] (see Methods for model details), and taking the average values of the lower end of the data envelopes shown in Supplementary Fig. S2, an upper estimate **can be obtained** for marine sulphate of ~1.0-6.6 mM for the interval from ~524 to ~514 Myr ago, followed by ~0.4-1.4 mM for ~514 to 512 Myr ago. These estimates are broadly consistent with previously modelled estimates of ~5-10 mM[24] and with fluid inclusion-based estimates of ~4.5-11 mM for the early Cambrian[26]. Thus, the early Cambrian ocean was characterized by a relative paucity of sulphate, when compared with the modern ocean (~28-29 mM). Our data document a significant drawdown of more than half of the sulphate pool during early Cambrian Stage 4 (~514-512 Myr ago), coincident with the BTE.

Environmental oxygenation and animal radiations

The covariant behaviour of the carbon and sulphur isotope systems during **Cambrian** Stage 2 to late Stage 3 can be explained by coupled burial of pyrite and organic carbon in marine sediments under highly productive, anoxic conditions[22,27,28]. Such conditions result in enhanced preservation and burial of organic carbon, and simultaneously enhance microbial sulphate reduction (MSR), leading to a high pyrite burial flux. Since pyrite and organic carbon are enriched in the lighter isotopes (^{32}S and ^{12}C respectively), elevated burial fluxes on a global scale would drive the positive excursions in seawater sulphate $\delta^{34}S$ and inorganic $\delta^{13}C$.

A biogeochemical box model[11,29,30] (see Methods for model details) was applied to test whether measured trends in S isotopes can be reproduced from the coupled burial of sulphur (as pyrite) and carbon (as organic carbon). The model infers the rate of organic carbon burial using the $\delta^{13}C$ record and an isotopic mass balance, while the rate of pyrite burial is calculated

by assuming a linear relationship with organic carbon burial, allowing prediction of $\delta^{34}S$ values. Results (Fig. 2c) show that both the amplitude of positive sulphur isotope excursions and their long-term trend from ~524-514 Ma can be replicated in this way. The model assumes that the isotopic composition of carbon and sulphur inputs ($\delta^{13}C_{in}$, $\delta^{34}S_{in}$), and the background carbon and sulphur cycle input fluxes through weathering and metamorphism remain constant. **Variations in these processes** may help to explain the slight drift **of the baseline $\delta^{34}S$** in model average predictions when compared to the **observed** $\delta^{34}S$ data. The shaded areas in Fig. 2 show the result of varying $\delta^{13}C_{in}$ between -5‰ and -8‰, allowing the model to encompass most of the data. Our model requires a low concentration of sulphate in seawater (best-fit shown is 1 mM), in order to match the rate and amplitude of $\delta^{34}S$ variations, consistent with the lower end of maximum estimates derived from the 'rate method' model.

The coupled carbon and sulphur isotope swings show **repeated cycles** of approximately **0.5**–2 Myrs duration that reflect cyclical changes in the burial rates of organic carbon and pyrite, which may be induced by **episodic** expansion of **bottom**-water anoxia/euxinia**.** Ultimately, coupled burial of both reduced species in the marine sediments results in the release of oxygen and other marine oxidants[13]. Each rising limb and the peak of the positive isotope swing thus represents enhanced net oxygen production **and** a pulse of atmospheric oxygen, which initially **increases the extent of oxygenated waters and/or the maximum dissolved O_2 in** the shallower marine realm. Subsequently, increased ventilation of the deep ocean would result in a lower flux **of reductant** (organic carbon and pyrite) to seafloor sediments[31]. This **acts to** decrease the net oxidant flux, which ultimately **buffers against further oxygenation. Furthermore, positive feedbacks may drive rapid bottom-water oxygenation, and in this case the decrease in the net oxidant flux may be substantial, leading to a** re-establish**ment of** anoxia, **and potentially** giving rise to the repetitive isotope cycles[32].

Alternatively, isotope cyclicity might be driven by orbital forcing via climatic impacts on weathering, as in the ~1–2 Ma "third-order" eustatic sequences of the Mesozoic and Cenozoic Eras[33]. However, neither the timing, duration and frequency of early Cambrian third-order sea-level fluctuations[17,34], nor regional sequence stratigraphy data from Siberia[35] (Supplementary Table S3), appear to match the isotope cycles identified in this study. Similarly, an erosional driver for the observed isotope cycles[36] is not compatible with

their combined high amplitude and frequency, and is not supported by contemporaneous changes in $^{87}Sr/^{86}Sr$[37]. Fluctuation in oxygen minimal zone depth[38,39], alongside biological feedbacks such as enhanced diurnal vertical migration via increased expansion of metazoan mobility[40], may also contribute to the perturbations in shallow ocean oxygenation.

To summarize, our model indicates the potential for large variations in the net **atmospheric** oxygen production flux (±50% around the baseline value; Fig. 2d). **We propose that periods of rising $\delta^{13}C$ represent enhanced burial of reductant and atmospheric oxygenation under an anoxic bottom-water condition, while the falling limbs record the decrease of reductant burial under a more widely oxygenated deep ocean.** A more direct estimate of oxygen production rates can be made within our model by treating both $\delta^{13}C$ and $\delta^{34}S$ as input parameters, thus inferring rates of organic carbon and pyrite burial, respectively, for the time points where we have input information for $\delta^{34}S$. These estimates are shown in Fig. 3 and are similar in magnitude to those of the carbon-only model, which is to be expected as the carbon-only model produced a reasonable fit to the $\delta^{34}S$ data.

One direct impact of pulses in atmospheric oxygenation during the early Cambrian was the episodic oxygenation of the marginal shallow marine environment. Shallow carbonate platforms, such as the early Cambrian Aldan-Lena rivers region, evidence relatively high animal origination rates and biodiversity[41,42]. Within shallow ocean ecosystems, biogenic reefs serve as critical evolutionary cradles and net sources of marine biodiversity[43]. Comparing the isotopic cycles and estimated oxygen production curves with species diversity curves for the Siberian Platform (see Supplementary information for full palaeontological data), oxygenation pulses (III, IV, V, VI, VII) generally coincide with regional biodiversity highs in either reef-building archaeocyathan or total animal species (Fig. 3). Although no significant total animal biodiversity high is associated with the oxygenation pulse IV, the number of archaeocyathan species increased dramatically by ~60%. Moreover, the rising limb of isotope excursion IV coincides with the first emergence of trilobites, bivalved arthropods, and stenothecoids possessing relatively thick biomineralised skeletons, as well as a geographic expansion of possible burrowing filter-feeding arthropods over the Siberian Platform, as recorded by the appearance of Thalassinoides-type trace fossils[35]. A significant increase in the beta-diversity of reefal palaeocommunities is also

restricted to the IV interval in the Aldan-Lena rivers region[2], reflecting a differentiation of species between assemblages, and thus ecological diversification within the shallow marine environment.

On a global scale, positive isotope excursion V coincides with major radiations of large predatory arthropods and radiodonts, increased durophagy, and the first appearance of pelagic motile deuterostomes, evidenced by the Chengjiang biota and similar faunas[44,45]. Similarly, excursion VII coincides with a global radiation of echinoderms and archaeocyaths. The latter is revealed by the gamma-diversity peak reflecting formation of numerous isolated faunal provinces[2]. By contrast, minor extinction events here and elsewhere appear to be associated with the negative excursions[17,44,46]. In the deeper ocean setting of northern Siberia and South China, multi-proxy analyses reveal broadly similar oceanic redox fluctuations[4,47–49], which appear to coincide with the positive carbon isotope excursions in the early Cambrian[15,46,50]. These episodic redox oscillations, which appear in the $\delta^{13}C$ record and, in places, as $\delta^{13}C$ and $\delta^{34}S$ covariance[15] (also see Supplementary Fig. S6 for $\delta^{13}C$-$\delta^{34}S$ covariance from the Cambrian Stage 2 ZHUjiaqing Carbon isotope Excursion (ZHUCE) in the Xiaotan section in South China), suggest that these coupled isotope excursions record a global phenomenon. We therefore propose that perturbations to shallow ocean oxygen budgets were driven by fluctuations in atmospheric oxygen. **This gave rise to higher oxygen levels required for various new animal body plans and lifestyles, and likely resulted in the geographic expansion/contraction of the habitable zone within shallow ocean ecosystems. This shallow ocean oxygen control is reflected in the fluctuations of animal origination and speciation rates, and thus regulated the global biodiversity radiation patterns of early Cambrian animals.**

Expanded shallow ocean anoxia and sulphate reduction across the BTE

In contrast to the coupling of carbon and sulphur isotopes during **Cambrian stages 2-3**, the **decoupled $\delta^{13}C$-$\delta^{34}S$ records and unsystematic** temporal fluctuations in $\delta^{34}S$ observed across the BTE (Fig. 1) appear to reflect a significant and persistent decline in oceanic sulphate concentration (Supplementary Fig. S2). At reduced marine residence times, $\delta^{34}S$ is more responsive to perturbations to the sulphur cycle. A fall in seawater sulphate concentration is generally assigned to enhanced evaporite deposition or widespread anoxia, and indeed, there

are a number of thick evaporite deposits in the global rock record during this period[51,52]. However, these evaporites are restricted to the innermost isolated basins of the Siberian Platform and the Australian part of Eastern Gondwana, respectively, and their stratigraphic distribution does not correlate with the interval of low sulphate inferred for the BTE. This suggests that anoxic/euxinic conditions likely prevailed in the Siberian shallow marine realm at this time. **The expansion of shallow ocean anoxia is consistent with an observed accumulation of over 750,000 km^2 of black organic-rich carbonate-rich sediments (comprising bituminous limestone, chert and argillaceous calcareous sapropelic shale) in the Sinsk Formation across the Siberian Platform, as well as enrichments in pyrite, V, As, Cr, Cu and Ni, and the presence of abundant biomarkers indicative of anaerobic bacteria as a major source of organic matter[20,53]. Such phenomena have previously** been linked to shoaling of oxygen-depleted waters during a major marine transgression[20,35], which has been suggested as the cause of the major extinction pulse of the BTE (Sinsk event; Fig. 1). **Thus, while bottom-water anoxia may contribute to the episodic burial of reductant and oxygenation of the atmosphere and shallow ocean in the Cambrian stages 2-3, shoaling of anoxic waters in the Cambrian Stage 4 may drive mass extinction, and therefore a reduction in primary productivity and overall reductant burial.**

Implications for early animal diversification

Oxygenation of the early Cambrian **shallow** marine environment can be inferred from the coupled behaviour of the carbon and sulphur cycles. Episodic **shallow ocean oxygenation** corresponds to pulses of animal diversification, and so provides a plausible environmental explanation for the step-wise nature of the Cambrian **radiation of animals**. In the modern **and ancient** oceans, well-oxygenated waters are generally associated with larger body sizes, higher diversity, advanced skeletal biomineralization and increased motility and carnivory[9,10,54,55]. Pulses of **shallow ocean** oxygenation in the early Cambrian likely expanded the global proportion of habitable **marginal** ocean to provide new ecological opportunities **and biodiversity cradles**. Similarly, the extended radiation of the Great Ordovician Biodiversification Event (~490-450 Ma) also appears to have been facilitated by pulses in atmospheric oxygenation[56]. A prolonged pause in biological diversification, which lasted over 20 million years and was associated with recurring extinctions (BTE, SPICE-trilobite extinctions[17]), occurred between these two major diversification events. Environmental

stress caused by the persistent development of oxygen-deficient conditions in shallow marine realms **due to low net atmospheric oxygen production**[57] is likely to have been a major contributing factor. Thus, the global extent of well-oxygenated **shallow ocean** habitats during the early Paleozoic**, as well as the maximum dissolved oxygen content of surface waters**, played a vital role in regulating the emergence and radiation of complex early animal life.

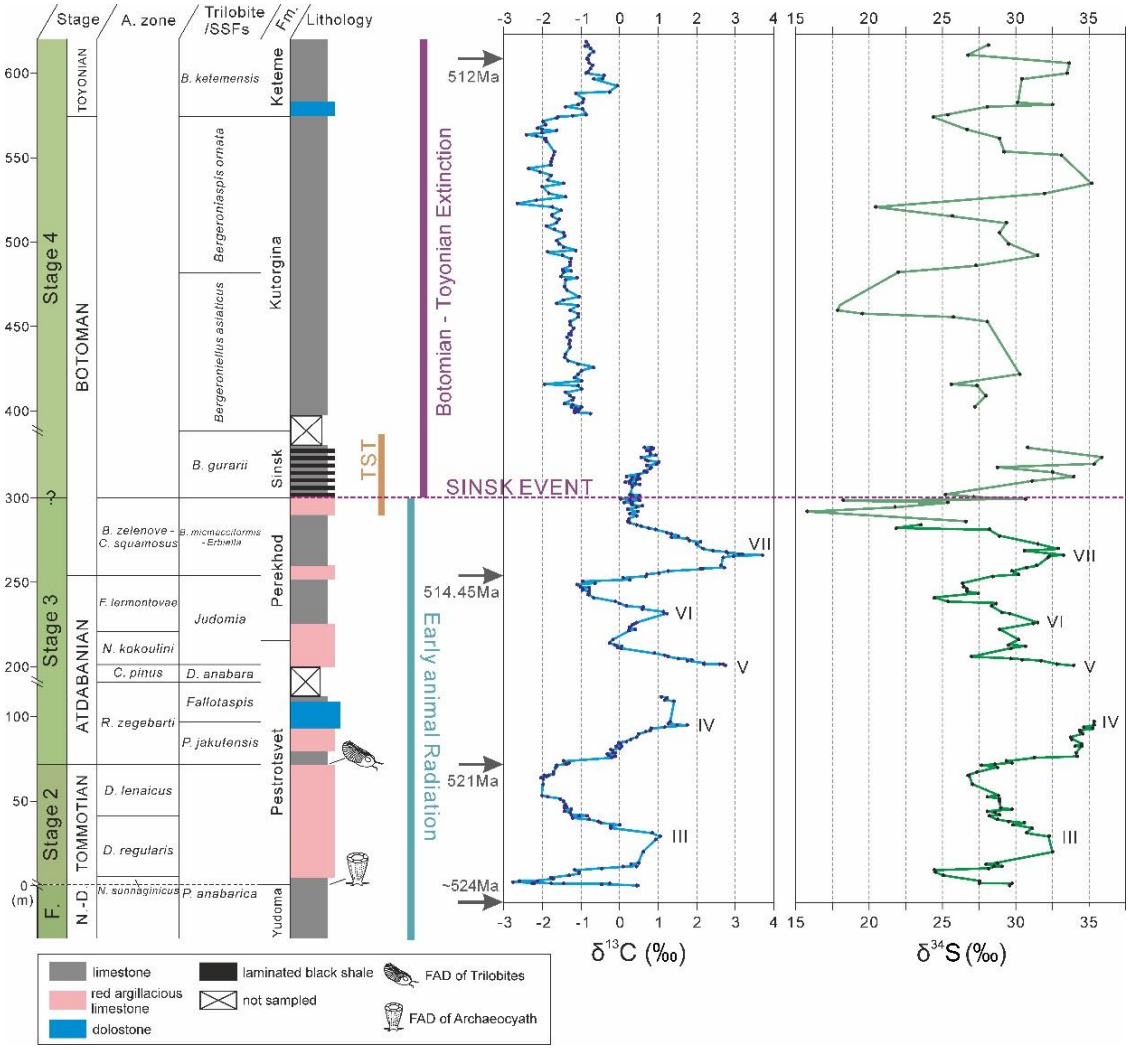

Fig. 1. High-resolution carbonate carbon ($\delta^{13}C$) and carbonate-associated sulphate sulphur isotope ($\delta^{34}S$) records from Cambrian Stage 2 to Stage 4 of Siberian Aldan-Lena rivers sections. Regional stage subdivisions are shown next to the global subdivision plan for comparison[14] (F.: Fortunian Stage; N.–D.: Nemakit–Daldynian Stage; TST: Transgressive System Tract[36]; Fm.: Formation; **A.: Archaeocyathan; SSFs: small shelly fossils**). Names for the positive $\delta^{13}C$ peaks (III, IV, V, VI, VII) are consistent with those of previously suggested $\delta^{13}C$ curves[14]. FAD: First appearance datum.

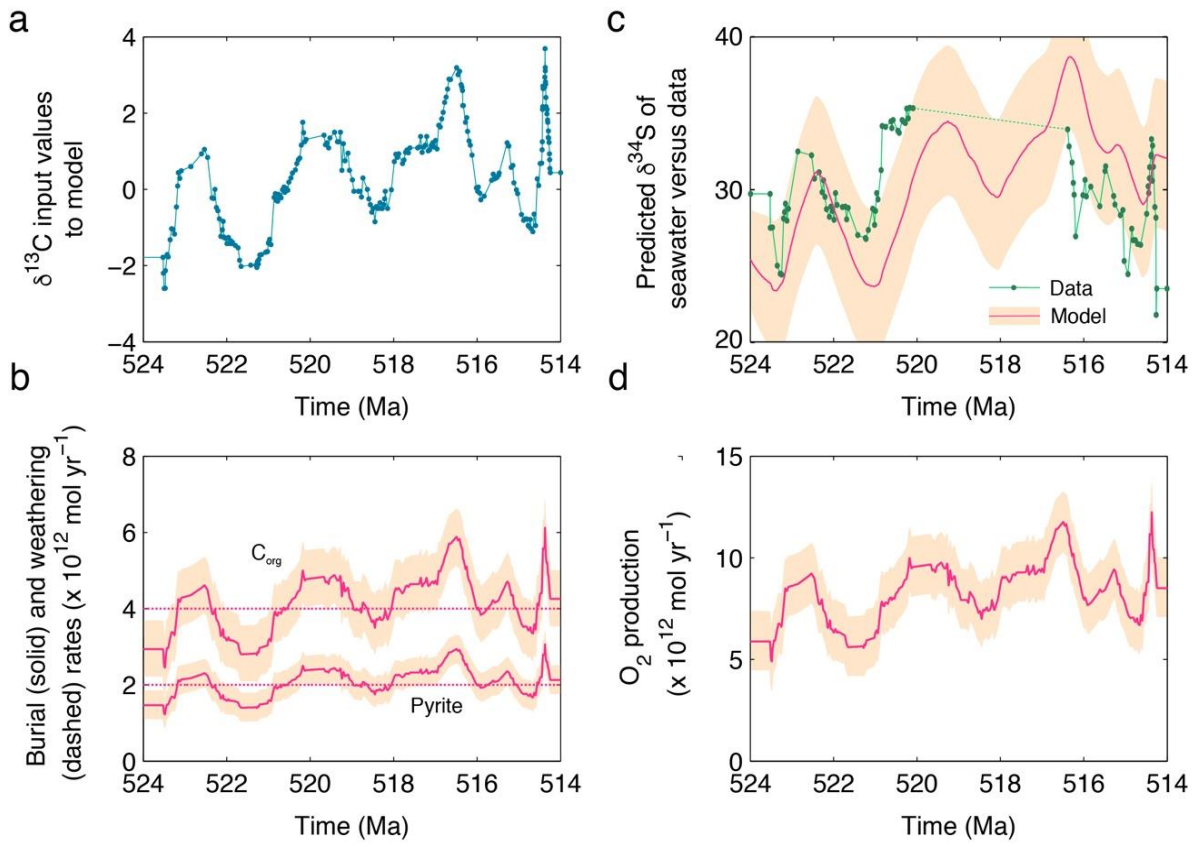

Fig. 2. Carbon and sulphur cycle model output. a. This model takes measured $\delta^{13}C$ as an input parameter. **b**. Burial rates of organic carbon (C_{org}) are inferred from isotope mass balance and $\delta^{13}C$ record, and burial rates of pyrite are assumed to be controlled by modelled organic matter availability. **c**. Comparison between analysed $\delta^{34}S$ data (green curve) and simulated seawater sulphate $\delta^{34}S$ value (pink); Dashed part of the green curve shows the sampling gap. **d**. Variations in modelled net oxygen production. For all plots, the uncertainty window represents an alteration of the $\delta^{13}C$ value of carbon inputs between -5‰ and -8‰.

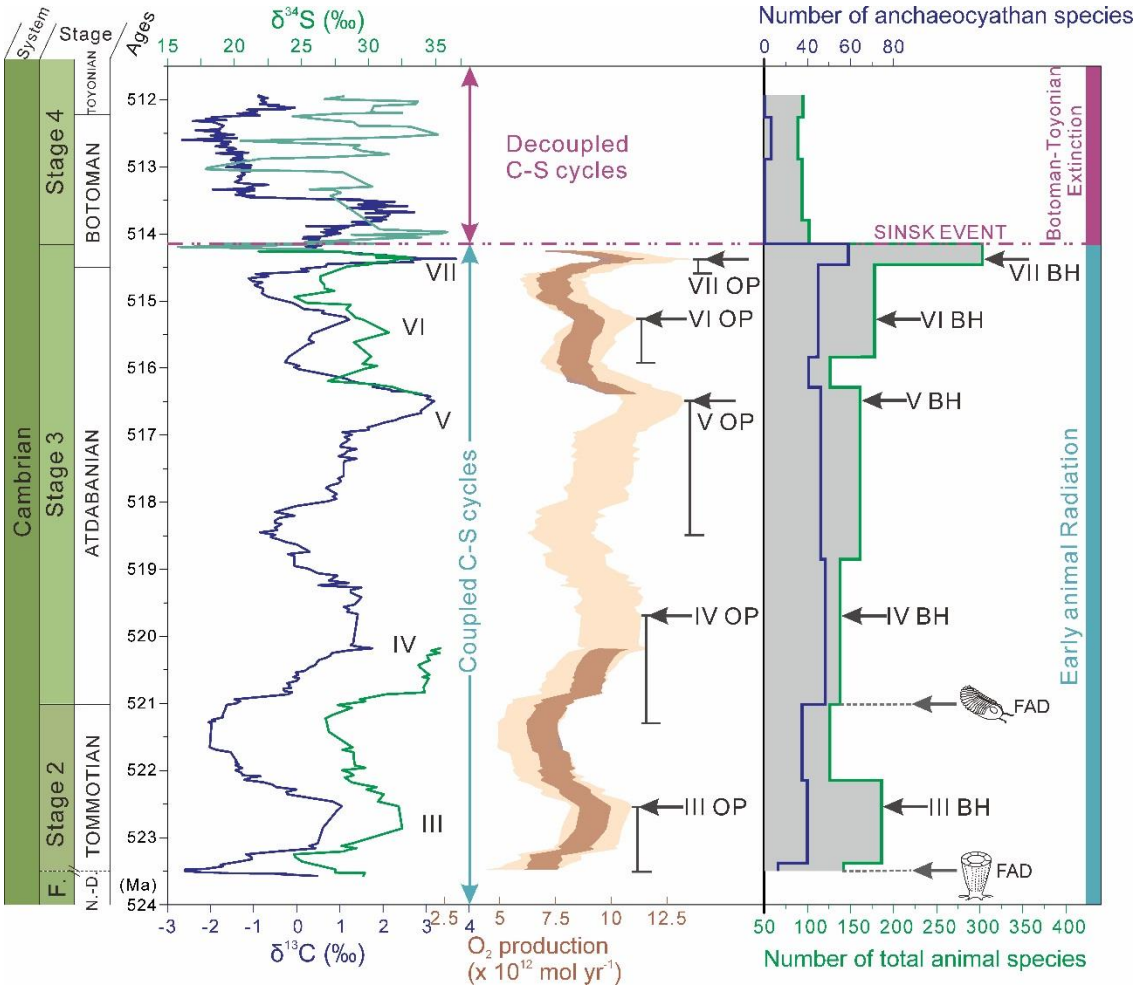

Fig. 3. Animal diversity, biological events and their correlation to the isotope records and oxygenation pattern across Cambrian stages 2-4. Global oxygen production is inferred from isotope mass balance modelling, using inputs of $\delta^{13}C$ only (light shade), or $\delta^{13}C$ and $\delta^{34}S$ (dark shade). **Archaeocyathan species (blue line) and total animal species (green line) diversity records are** expressed as the mean number of species per sampling unit (grey box) in Siberia; OP: oxygenation pulse; F.: Fortunian Stage; N.–D.: Nemakit–Daldynian Stage. FAD: First appearance datum.

References

1. Erwin, D. H. *et al.* The Cambrian conundrum: early divergence and later ecological success in the early history of animals. *Science.* **334,** 1091–1097 (2011).

2. **Zhuravlev, A. Yu. & Naimark, E. B. Alpha, beta, or gamma: Numerical view on the Early Cambrian world. *Palaeogeogr. Palaeoclimatol. Palaeoecol.* 220, 207–225 (2005).**

3. **Na, L. & Kiessling, W. Diversity partitioning during the Cambrian radiation. *Proc. Natl. Acad. Sci.* 112, 201424985 (2015).**

4. Boyle, R. A. *et al.* Stabilization of the coupled oxygen and phosphorus cycles by the evolution of bioturbation. *Nat. Geosci.* **7,** 671–676 (2014).

5. Lenton, T. M., Boyle, R. A., Poulton, S. W., Shields-Zhou, G. A. & Butterfield, N. J. Co-evolution of eukaryotes and ocean oxygenation in the Neoproterozoic era. *Nat. Geosci.* **7,** 257–265 (2014).

6. Chen, X. *et al.* Rise to modern levels of ocean oxygenation coincided with the Cambrian radiation of animals. *Nat. Commun.* **6,** 7142 (2015).

7. Mills, D. B. *et al.* Oxygen requirements of the earliest animals. *Proc. Natl. Acad. Sci.* **111,** 4168–4172 (2014).

8. Zhang, S. *et al.* Sufficient oxygen for animal respiration 1,400 million years ago. *Proc. Natl. Acad. Sci.* **113,** 1731–1736 (2016).

9. Sperling, E. A. *et al.* Oxygen, ecology, and the Cambrian radiation of animals. *Proc. Natl. Acad. Sci.* **110,** 13446–13451 (2013).

10. **Levin, L. A., Gage, J. D., Martin, C. & Lamont, P. A. Macrobenthic community structure within and beneath the oxygen minimum zone, NW Arabian Sea. *Deep Sea Res. Part II Top. Stud. Oceanogr.* 47, 189–226 (2000).**

11. Berner, R. A. GEOCARBSULF: A combined model for Phanerozoic atmospheric O_2 and CO_2. *Geochim. Cosmochim. Acta* **70,** 5653–5664 (2006).

12. Kump, L. R. & Garrels, R. M. Modeling atmospheric O_2 in the global sedimentary redox cycle. *Am. J. Sci.* **286,** 337–360 (1986).

13. Saltzman, M. R. *et al.* Pulse of atmospheric oxygen during the late Cambrian. *Proc. Natl. Acad. Sci.* **108,** 3876–3881 (2011).

14. Brasier, M. D., Corfield, R. M., Derry, L. A., Rozanov, A. Yu. & Zhuravlev, A. Yu. Multiple $\delta^{13}C$ excursions spanning the Cambrian explosion to the Botomian crisis in Siberia. *Geology* **22,** 455 (1994).

15. Dahl, T. W. *et al.* Reorganisation of Earth's biogeochemical cycles briefly oxygenated

the oceans 520 Myr ago. *Geochemical Perspect. Lett.* **3,** 210–220 (2017).

16. Maloof, A. C. *et al.* The earliest Cambrian record of animals and ocean geochemical change. *Geol. Soc. Am. Bull.* **122,** 1731–1774 (2010).

17. Peng, S., Babcock, L. E. & Cooper, R. A. The Cambrian Period. in *The Geologic Time Scale 2012* (eds. Gradstein, F. M., Ogg, J. G., Schmitz, M. D. & Ogg, G. M.) 437–488 (Elsevier Science Limited, 2012).

18. Tostevin, R. *et al.* Constraints on the late Ediacaran sulfur cycle from carbonate associated sulfate. *Precambrian Res.* **290,** 113–125 (2017).

19. Cui, H. *et al.* Redox-dependent distribution of early macro-organisms: Evidence from the terminal Ediacaran Khatyspyt Formation in Arctic Siberia. *Palaeogeogr. Palaeoclimatol. Palaeoecol.* **461,** 122–139 (2016).

20. Zhuravlev, A. Yu. & Wood, R. A. Anoxia as the cause of the mid-early Cambrian (Botomian) extinction event. *Geology* **24,** 311 (1996).

21. Bambach, R. K. Phanerozoic Biodiversity Mass Extinctions. *Annu. Rev. Earth Planet. Sci.* **34,** 127–155 (2006).

22. Gill, B. C., Lyons, T. W. & Saltzman, M. R. Parallel, high-resolution carbon and sulfur isotope records of the evolving Paleozoic marine sulfur reservoir. *Palaeogeogr. Palaeoclimatol. Palaeoecol.* **256,** 156–173 (2007).

23. Veizer, J., Holser, W. & Wilgus, C. Correlation of $^{13}C/^{12}C$ and $^{34}S/^{32}S$ secular variations. *Geochim. Cosmochim. Acta* **44,** 579–587 (1980).

24. Algeo, T. J., Luo, G. M., Song, H. Y., Lyons, T. W. & Canfield, D. E. Reconstruction of secular variation in seawater sulfate concentrations. *Biogeosciences* **12,** 2131–2151 (2015).

25. Kah, L. C., Lyons, T. W. & Frank, T. D. Low marine sulphate and protracted oxygenation of the Proterozoic biosphere. *Nature* **431,** 834–838 (2004).

26. Brennan, S. T., Lowenstein, T. K. & Horita, J. Seawater chemistry and the advent of biocalcification. *Geology* **32,** 473 (2004).

27. Berner, R. A. Sedimentary pyrite formation: An update. *Geochim. Cosmochim. Acta* **48,** 605–615 (1984).

28. Gill, B. C. *et al.* Geochemical evidence for widespread euxinia in the Later Cambrian ocean. *Nature* **469,** 80–83 (2011).

29. Garrels, R. M. & Lerman, A. Coupling of the sedimentary sulfur and carbon cycles; an improved model. *Am. J. Sci.* **284,** 989–1007 (1984).

30. Bergman, N. M. COPSE: A new model of biogeochemical cycling over Phanerozoic time. *Am. J. Sci.* **304,** 397–437 (2004).

31. Algeo, T. J. & Ingall, E. Sedimentary C_{org}:P ratios, paleocean ventilation, and Phanerozoic atmospheric pO_2. *Palaeogeogr. Palaeoclimatol. Palaeoecol.* 256, 130–155 (2007).

32. Handoh, I. C. & Lenton, T. M. Periodic mid-Cretaceous oceanic anoxic events linked by oscillations of the phosphorus and oxygen biogeochemical cycles. *Global Biogeochem. Cycles* 17, 1–11 (2003).

33. Boulila, S. *et al.* On the origin of Cenozoic and Mesozoic "third-order" eustatic sequences. *Earth-Science Rev.* 109, 94–112 (2011).

34. Haq, B. U. & Schutter, S. R. A Chronology of Paleozoic Sea-Level Changes. *Science.* 322, 64–68 (2008).

35. Zhuravlev, A. Yu. Outlines of the Siberian platform sequence stratigraphy in the Lower and lower Middle Cambrian (Lena-Aldan area). *Rev. Española Paleontol.* 105–114 (1998).

36. Shields, G. A. & Mills, B. J. W. Tectonic controls on the long-term carbon isotope mass balance. *Proc. Natl. Acad. Sci.* 114, 4318–4323 (2017).

37. Derry, L. A., Brasier, M. D., Corfield, R. M., Rozanov, A. Yu. & Zhuravlev, A. Yu. Sr and C isotopes in Lower Cambrian carbonates from the Siberian craton: A paleoenvironmental record during the 'Cambrian explosion'. *Earth Planet. Sci. Lett.* 128, 671–681 (1994).

38. Feng, L., Li, C., Huang, J., Chang, H. & Chu, X. A sulfate control on marine mid-depth euxinia on the early Cambrian (ca. 529–521Ma) Yangtze platform, South China. *Precambrian Res.* 246, 123–133 (2014).

39. Guilbaud, R. *et al.* Oxygen minimum zones in the early Cambrian ocean. *Geochemical Perspect. Lett.* 33–38 (2018).

40. Butterfield, N. J. Oxygen, animals and aquatic bioturbation: An updated account. *Geobiology* 16, 3–16 (2018).

41. Jablonski, D., Sepkoski, J. J., Bottjer, D. J. & Sheehan, P. M. Onshore-Offshore Patterns in the Evolution of Phanerozoic Shelf Communities. *Science.* 222, 1123–1125 (1983).

42. Zhuravlev, A. Yu. & Wood, R. A. The two phases of the Cambrian Explosion. *Sci. Rep.* 8, 1–10 (2018).

43. Kiessling, W., Simpson, C. & Foote, M. Reefs as Cradles of Evolution and Sources of Biodiversity in the Phanerozoic. *Science.* 327, 196–198 (2010).

44. Zhu, M.-Y., Babcock, L. E. & Peng, S.-C. Advances in Cambrian stratigraphy and paleontology: Integrating correlation techniques, paleobiology, taphonomy and paleoenvironmental reconstruction. *Palaeoworld* **15,** 217–222 (2006).

45. Bicknell, R. D. C. & Paterson, J. R. Reappraising the early evidence of durophagy and drilling predation in the fossil record: implications for escalation and the Cambrian Explosion. *Biol. Rev.* **93,** 754–784 (2018).

46. Wang, D. *et al.* Coupling of ocean redox and animal evolution during the Ediacaran-Cambrian transition. *Nat. Commun.* 9, 2575 (2018).

47. Jin, C. *et al.* A highly redox-heterogeneous ocean in South China during the early Cambrian (~529–514 Ma): Implications for biota-environment co-evolution. *Earth Planet. Sci. Lett.* 441, 38–51 (2016).

48. Zhang, J. *et al.* Heterogenous oceanic redox conditions through the Ediacaran-Cambrian boundary limited the metazoan zonation. *Sci. Rep.* 7, 8550 (2017).

49. Zhang, L. *et al.* The link between metazoan diversity and paleo-oxygenation in the early Cambrian: An integrated palaeontological and geochemical record from the eastern Three Gorges Region of South China. *Palaeogeogr. Palaeoclimatol. Palaeoecol.* 495, 24–41 (2018).

50. Wei, G.-Y. *et al.* Marine redox fluctuation as a potential trigger for the Cambrian explosion. *Geology* 46, 1–5 (2018).

51. Kovalevych, V., Marshall, T., Peryt, T., Petrychenko, O. & Zhukova, S. Chemical composition of seawater in Neoproterozoic: Results of fluid inclusion study of halite from Salt Range (Pakistan) and Amadeus Basin (Australia). *Precambrian Res.* **144,** 39–51 (2006).

52. Astashkin, V. A. *et al*. Cambrian System on the Siberian Platform. Correlation chart and explanatory notes. *Int. Union Geol. Sci. Publ.* 1–133 (1991).

53. Parfenova, T. M., Korovnikov, I. V., Eder, V. G. & Melenevskii, V. N. Organic geochemistry of the Lower Cambrian Sinyaya Formation (northern slope of the Aldan anteclise). *Russ. Geol. Geophys.* 58, 586–599 (2017).

54. Tostevin, R. *et al.* Low-oxygen waters limited habitable space for early animals. *Nat. Commun.* 7, 12818 (2016).

55. Payne, J. L. *et al.* The evolutionary consequences of oxygenic photosynthesis: A body size perspective. *Photosynth. Res.* 107, 37–57 (2011).

56. Edwards, C. T., Saltzman, M. R., Royer, D. L. & Fike, D. A. Oxygenation as a driver of the Great Ordovician Biodiversification Event. *Nat. Geosci.* **10,** 925–929 (2017).

57. Krause, A. J. *et al.* Stepwise oxygenation of the Paleozoic atmosphere. *Nat. Commun.* 9, 4081 (2018).

Acknowledgements

This work was supported by National Natural Science Foundation of China (41661134048) and Strategic Priority Research Program (B) of the Chinese Academy of Sciences (XDB18000000) to M.Z., NERC (NE/1005978/1 and NE/P013643/1) to G.A.S., University of Leeds Academic Fellowship to B.J.W.M., ERC Consolidator grant 682760 (CONTROLPASTCO2) to P.A.E.PvS, NERC (NE/N018559/1) to S.W.P., University College London Overseas Research Scholarship to T.H.. We acknowledge G. Tarbuck and D. Hughes for assistance in the geochemical analysis. We thank T. W. Dahl, B. S. Wade, **R. Newton**, C. Yang and **L. Yao** for valuable discussions. **We thank T. Algeo, B. Gill and an anonymous reviewer for constructive comments.**

Author contributions

T.H., M.Z., and G.A.S. conceived the project. G.A.S., P.A.E.PvS. and **B.J.W.M.** supervised the project. M.Z., A.Y. and A.Yu.Z. collected the samples. T.H. and P.M.W. analysed the samples. A.Yu.Z. provided the fossil data. B.J.W.M. and T.H. created the models. All authors contributed to data interpretation and the writing of the manuscript.

Competing interests

The authors declare no competing interests.

Additional information

Correspondence and requests for materials should be addressed to T.H. (T.He@leeds.ac.uk)

Methods

Carbonate-associated sulphate (CAS) extraction and $\delta^{34}S$ analysis. Large blocks (>200 g) of carbonate were cut and polished under running water, in order to trim weathered surfaces prior to powdering. Blocks were then cut into small chips using a water-cooled, diamond tipped bench circular saw. Rock chips were then ground to a fine powder (flour-like consistency, <10 µm) using a *Retsch*® Agate Mortar grinder. We applied a high-fidelity miniaturized CAS extraction protocol, which is an extension of two published approaches[39,40]. The protocol was established following tests involving twelve-times consecutive leaching of five carbonate samples from different stratigraphic horizons of the Aldan-Lena river sections and three samples from the Ediacaran Nama Group[18]. Approximately 10 g of the fine powder for each sample was leached in 40 ml of 10% NaCl solution for 24 hours to remove the non-CAS sulphur-bearing compounds or easily soluble sulphate. During leaching, samples were constantly agitated using a roller shaker at room temperature. Residues were rinsed in ultrapure water 3 times between each leach and 5 times after the final leach. After each leach, the leachate was retained, and the presence of sulphate was tested by adding saturated barium chloride solution for 3 days to precipitate barite. As illustrated in Supplementary Fig. S3, the amount of sulphur removed during sequential NaCl leaching of test samples exhibited a sharp decline through multiple NaCl leaches and reached blank levels in the 3rd or 4th leachates, suggesting five leaches is sufficient for complete removal of soluble sulphur-bearing constituents from ~10 g of carbonate powder. All pre-leached carbonate samples were treated with 6 M HCl, which was added in calculated aliquots based on total HCl-leachable carbonate content. This step was completed within 30 minutes to minimise the potential for pyrite oxidation during dissolution. The insoluble residue was separated from the solution by centrifugation in 50 ml tubes followed by filtration through *VWR*® 0.2 µm Polypropylene membrane syringe filters. Saturated barium chloride solution was then added to the filtered solution and left to precipitate within the housing of a sealed tube over 3 days at room temperature. In cases where no visible precipitates were seen in the solution after 24 h, 2 mg isotopic-grade sulphur-free quartz powder was added, which served as an inert medium onto which barium sulphate could precipitate[40]. Each sample was centrifuged, and the supernatant replaced with ultrapure water repeatedly until the pH attained neutral values. Washed samples were then dried prior to isotope analysis. $^{34}S/^{32}S$ analysis of barium

sulphate precipitates was undertaken using an *Elementar*® Pyrocube elemental analyzer linked to *Isoprime*® 100 mass spectrometer operated in continuous flow mode at the Lancaster Environment Centre, Lancaster University. Pellets of $BaSO_4$, resulting from sulphate extraction with or without the addition of quartz powder, were combusted in tin capsules in the presence of excess vanadium pentoxide (V_2O_5) at 1030°C to yield SO_2 for the determination of $\delta^{34}S$. All samples and standards were matrix matched, and values were corrected against VCDT using within-run analyses of international standards NBS-127 and SO5 (assuming $\delta^{34}S$ values of +20.3‰ and +0.49‰, respectively). Within-run standard replication was below 0.3‰ (1sd). Procedural standard solutions of calcium sulphate precipitated as barium sulphate were used to test the integrity of the method[40]. These yielded $\delta^{34}S$ values of +2.7‰ (0.3‰, 1sd, n=12) compared to values of +3.0‰ (0.3‰, 1sd, n=13) for analysis of the raw calcium sulphate powder. Blank contamination associated with $\delta^{34}S$ determination was zero.

CAS concentrations and sulphur content in NaCl leached solution.

The concentration of CAS and sulphur content in different leaching steps were measured in aliquots of the filtered solution using a *Varian*® 720 Inductively Coupled Plasma Optical Emission Spectrometer (ICP-OES) at the London Geochemistry and Isotope Centre (LOGIC), University College London. Wavelength 182.5 nm was selected to minimise interference with calcium ions, and analysis was conducted using the N_2-purging polyboost function to avoid oxygen interference in the system.

Carbonate carbon and oxygen isotopes. About 20 mg of rock powder that was drilled from a rock chip was analyzed for stable C and O isotopes. Limestone samples were reacted with 100% H_3PO_4 at 25°C for more than 12 h, and dolostone samples were reacted with 100% H_3PO_4 at 50°C for more than 24 h. Prepared gas samples were analysed for $^{13}C/^{12}C$ and $^{18}O/^{16}O$ using the Chinese national standard, an Ordovician carbonate from a site near Beijing (reference number GBW04405: $\delta^{13}C$= 0.57 ± 0.03‰ VPDB; $\delta^{18}O$= -8.49 ± 0.13‰ VPDB). The analyses were performed using the *Finnigan*® MAT 253 mass spectrometers at the Nanjing Institute of Geology and Palaeontology, Chinese Academy of Sciences.

Elemental analysis. For concentrations of diagenesis-diagnostic elements, including Ca, Mg, Mn, and Sr, an aliquot of approximately 50 mg of the rock power was micro-drilled from a rock chip and dissolved with excess 6 M hydrochloric acid at room temperature for 12 h. The concentration of the acid used here is identical to the one used for CAS extraction after NaCl leaching. The reaction was facilitated using an ultrasonic bath and roller shaker. After centrifugation, aliquots of the supernatant were then analysed for elemental concentration using the *Varian*® 720 ICP-OES at University College London. All analyses for elements were monitored using certified reference materials: SRM1c (argillaceous limestone), SRM120b (Florida phosphate rock). Solution standards were run at the start of the analyses along with a blank to monitor the accuracy of the bulk elemental analysis. Laboratory control solution standards were also run after every batch of 20 samples to monitor drift and precision. Analytical precision for elemental concentrations was generally better than 5%.

'Rate method' model. Maximum seawater sulphate concentrations are calculated using the modified 'rate method'[24,25]. The model was constructed based on the observed rate of change in seawater sulphate (carbonate-associated sulphate) $\delta^{34}S$, fractionation between oxidized (sulphate) and reduced sulphur (pyrite) reservoirs and equation (1) that connects the two parameters, where F_x represents the input and output fluxes, $\Delta^{34}S_x$ represents isotopic difference of $\delta^{34}S$ between fluxes (Q = total input flux of sulphur, SUL = seawater sulphate, PY = pyrite burial, SW = seawater/sulphate deposition) and M_{SW} represents the mass of sulphate in the ocean.

$$\frac{d\delta^{34}S}{dt} = \frac{\left(\left(F_Q \times \Delta^{34}S_{Q-SW}\right) - \left(F_{PY} \times \Delta^{34}S_{SUL-PY}\right)\right)}{M_{SW}} \quad (1)$$

The maximum rates of $\delta^{34}S$ change are attained when sulphur input flux to the ocean approaches zero ($F_Q = 0$), and the standing oceanic sulphate reservoir is removed as pyrite. Equation (1) is then transformed to equation (2) to calculate the size of seawater sulphate reservoir.

$$M_{SW} = \frac{F_{PY} \times \Delta^{34}S_{SUL-PY}}{\frac{d\delta^{34}S}{dt}} \quad (2)$$

Because the observed rates of seawater sulphate $\delta^{34}S$ change in a normal marine environment should never exceed the theoretical maximum rates of change ($d\delta^{34}S/dt$), the

calculation of M_{SW} using equation (2) should provide the maximum estimate of seawater sulphate concentration. The definition of F_{PY}, $\Delta^{34}S_{SUL\text{-}PY}$, and unit-conversion constants (gram to mM) are consistent with the values applied for the long-term secular variation study of seawater sulphate concentration[24]. $F_{PY} = 4 \times 10^{13}$ g yr^{-1} is suggested for a normal marine environment. $\Delta^{34}S_{SUL\text{-}PY} = 35‰$ is suggested for the fractionation during MSR. The variation of seawater sulphate concentration ($[SO_4^{2-}]$) between ~524 Myr ago and ~512 Myr ago is represented based on a point-to-point calculation (Supplementary Fig. S2). Because the sampling density between $\delta^{34}S$ values is generally below 0.1 Myr (Supplementary Table S3), this study utilises a 0.1-Myr gridded data smoothing curve (red line in Supplementary Fig. S2) as representing the best estimate of seawater $[SO_4^{2-}]$. Besides, the maximum concentration for an individual point could be under or overestimated due to fluctuations and anomalies in the rate of $\delta^{34}S$ changes. To overcome this bias, the resulting $[SO_4^{2-}]$ data are binned into 0.5-Myr bands. The lower envelope (black dotted line in Supplementary Fig. S2) of the $[SO_4^{2-}]$ red curve, which links the lowest value for each band, is expected to represent the maximum rates of $\delta^{34}S$ change and thus the theoretical estimate of maximum seawater sulphate concentration through time.

Coupled carbon and sulphur cycle model. A simple model of the global carbon and sulphur cycles was applied to explore the proposed mechanisms for isotopic variations in the system. This follows the work of Garrels and Lerman[29], Berner[11] and Bergman *et al*.[30]. The model calculates the global rate of organic carbon burial using isotope mass balance, and then attempts to predict the operation of the sulphur system based on the supply of organic matter. Supplementary Fig. S4 shows the model processes as a diagram; Supplementary Table S2 shows the model flux and parameter values. The model estimates long-term fluxes between the ocean and sediments for both carbon and sulphur. Carbon is modelled as CO_2 in the atmosphere and ocean (A), and will be buried either as organic carbon (G) or carbonate (C). Similarly, sulphur can exist as oceanic sulphate (S), and will be buried as pyrite (PYR) or gypsum (GYP). Weathering (and metamorphism) constitutes the return flux from the sediments to the ocean and atmosphere. We set the weathering inputs to constant values, which are chosen in line with previous models[11,30]. We allow for around half of present total organic carbon burial (and weathering) due to the absence of land plants, and an enhanced burial flux of pyrite sulphur due to anoxia. The weathering rate of gypsum is held constant,

but the burial rate is adjusted so that the model maintains a constant sulphate concentration. Due to the relatively short model timeframe relative to the residence times of the vast sedimentary reservoirs, these reservoirs are assumed to have a fixed isotopic composition and are assumed not to vary in size. The ocean and atmosphere reservoirs are allowed to vary in size and isotopic composition. Organic carbon burial is calculated via isotope mass balance[11,29], which uses the total carbon input fluxes and isotopic composition of seawater (δA) to calculate the required burial rate of isotopically depleted organic carbon (equation (3)):

$$B(G) = \frac{1}{\Delta B}\{ W(G)(\delta A - \delta G) + W(C)(\delta A - \delta C)\} \quad (3)$$

It is assumed that pyrite burial is governed by the supply rate of organic carbon to microbial sulphate reducers, and therefore scales with the burial rate of organic carbon (equation (4)). The proportionality constant (0.5) is chosen to balance pyrite weathering.

$$B(PYR) = 0.5\, B(G) \quad (4)$$

Variation in the ocean and atmosphere carbon is calculated as:

$$\frac{dA}{dt} = W(G) + W(C) - B(G) - B(C) \quad (5)$$

Variation in ocean sulphate is calculated as:

$$\frac{dS}{dt} = W(PYR) + W(GYP) - B(PYR) - B(GYP) \quad (6)$$

Variation in the isotopic composition of ocean sulphate is calculated as:

$$\frac{d(S \times \delta S)}{dt} = W(PYR)\delta PYR + W(GYP)\delta GYP - B(PYR)(\delta S - \Delta S) - B(GYP)\delta S \quad (7)$$

Net oxygen production flux is calculated from the burial rate of organic carbon and pyrite:

$$FO_2 = B(G) + 2 \cdot B(PYR) \quad (8)$$

The model is solved in MATLAB using the ODE (Ordinary Differential Equation) suite. The model broadly reproduces the duration and magnitude of fluctuations in $\delta^{34}S$ (Fig. 2c). It also predicts similar fluctuations in oxygen production (Fig. 2d). The model does not calculate the concentration of oxygen in the atmosphere and ocean, and all fluxes are assumed to be oxygen-independent. More detailed modelling, which takes into account the variation in oxygen sinks, is required to analyse the overall long-term trends in atmospheric oxygen levels.

An alternative version of the model is run in Fig. 3 that estimates pyrite burial rates directly from the $\delta^{34}S$ record. In this version, equation (4) is replaced by equation (9), and equation (7) is not required.

$$B(PYR) = \frac{1}{\Delta S}\{W(PYR)(\delta S - \delta PYR) + W(GYP)(\delta S - \delta GYP)\} \quad (9)$$

Total marine animal species diversity. Supplementary Table S4 shows the distribution and diversity of total and individual animal species of Cambrian stages 2-4 of the Siberian Platform. This dataset is an upgrade of a previously published version[20] **(see supplementary information for detailed description and source of data)**. Siberian biozones (archaeocyathids/trilobite) are selected as the sampling units for diversity data collection. The finalised animal diversity record is generated by plotting total species diversity against sampling units (grey boxes in Fig. 3).

Code availability.

The code used to generate the Coupled carbon and sulphur cycle model results is available from the corresponding author (T.He@leeds.ac.uk) on request.

Data availability.

The authors declare that data supporting the findings of this study are available within the article and Supplementary Tables S1–S4.

References

58. Wotte, T., Shields-Zhou, G. A. & Strauss, H. Carbonate-associated sulfate: Experimental comparisons of common extraction methods and recommendations toward a standard analytical protocol. *Chem. Geol.* **326–327,** 132–144 (2012).

59. Wynn, P. M., Fairchild, I. J., Baker, A., Baldini, J. U. L. & McDermott, F. Isotopic archives of sulphate in speleothems. *Geochim. Cosmochim. Acta* **72,** 2465–2477 (2008).